Project Acronym:

FUSROBOT(ENTERPRISES/0618/0016)

MRI-guided focused ultrasound robotic system for preclinical research.

Deliverable number: 4.1

Title: MRI compatibility of the transducer and robotic system.

Prepared by:

Theocharis Drakos (MEDSONIC)
Marinos Giannakou (MEDSONIC)
Christakis Damianou (CUT)
Leonidas Ioannou (YGIA POLYCLINIC)

Date: 23/04/2020

Table of Contents

Executive summary 3
Introduction 4
Materials and Methods 7
MR compatibility of the transducer 9
MR compatibility of the robotic device, ultrasonic piezoelectric motors and optical encoders 12
Non-Uniformity Index of agar-based phantom and MR-phantom under different configurations 16
Conclusions 19
References 20

Executive summary

In this deliverable (D4.1), the MR compatibility of the transducer and the robotic system was evaluated. Initially, a review of MR compatibility of various robotic systems that have been produced worldwide is described. Ultrasonic motors, encoders and transducers have been evaluated for MR compatibility. The MR sequences which were used to test the MR compatibility of different electronic devices are also mentioned.

The MR compatibility of the transducer was assessed using Fast Spoiled Gradient (FSPGR) sequence and the MR compatibility of the robotic system was assessed using T2 Weighted-Fast Relaxation Fast Spin Echo (T2W-FRFSE), FSPGR and Echo Planar Imaging (EPI) sequences. Because of the use of piezoelectric motors, transducer and optical encoders that require electricity during operation, the proposed robotic system was classified as MRI-conditional, according to the ASTM standards (F2503, F2052, F2213, F2182, and F2119).

The SNR in a specific location in the agar-based phantom was measured for transducer activation and the SNR in a specific location in an MR-phantom was also measured for different configurations (robotic device in MR bore, connection of robotic device with piezoelectric motors and optical encoders and activation of these devices). All components (piezoelectric motor, optical encoder and transducer) require the use of electricity during activation. The uniformity of the agar-based phantom and the MR quality assurance phantom was estimated for the different configurations.

Introduction

Overview of MR compatibility of MRI devices

A robotic system that is intended to work in MRI must be MR compatible for many reasons such as MR safety, preservation of image quality, and ability to operate unaffected by the scanner's electromagnetic fields [1]. The image quality needs to be high in order to obtain accurate results. The monitoring of temperature change in real-time at the treatment location where necrosis might be occurred is an important point using focused ultrasound under MRI guidance. An accurate temperature change can be recorded only if the image quality of the acquired MR images is sufficient for proper image processing using MR thermometry.

Any ferromagnetic material must be avoided entirely since this type of materials causes image artifacts and distortion [2]. Non-ferromagnetic metals such as aluminum, brass, titanium, high strength plastic, and composite materials are permissible, but they might cause imaging artifacts due to their interactions with the MR field gradients [3]. Acrylonitrile Butadiene Styrene (ABS) and other three-dimensional printing materials are MR compatible [4].

MR image artifacts may be caused due to the use of piezoelectric based-actuators. Piezoelectric actuators have been used extensively for MRI applications and have been shown to be MR compatible. Various types of MR compatible piezoelectric-based actuators have been developed and have been used in MRI guided therapeutic applications [5,6]. The motion of medical robots is performed via the actuators and each degree of freedom (DOF) needs an encoder (linear or rotational) that works as detector of the motion. During the motion of a robotic system, the encoders and the signals that are transferred via a cable can create artifacts and distort or shift the MR images by decreasing the homogeneity of the magnetic field. Moreover, the activation of the focused ultrasound transducer might cause artifacts to the MR images.

An MRI medical robotic system can be tested for MRI-compatibility by evaluating the effect of the stage on image artifacts, Signal-to-Noise Ratio (SNR), and magnetic field (B0) homogeneity. The use of each stage in the MRI scanner is evaluated with different pulse sequences. Proper attention to materials used in device design, electronic shielding and object placement, location, and orientation in the MR field can help control the effects of imaging artifacts. According to the U.S Food and Drug Administration (FDA) and the American Society for Testing and Materials (ASTM), three levels of MRI device classification are defined [7,8] as MR safe (safe to use in all MR environments), MR unsafe (poses a risk to the patient or the operator) and MR conditional (safe to use in a specific MR-environment).

The MR compatibility can be evaluated based upon changes in SNR. SNR is the signal in the center of the homogeneous phantom or tissue, divided by the noise intensity in the periphery as defined by the National Electrical Manufacturers Association (NEMA) standard for determining SNR in MR images [9]. The signal is defined as the mean pixel intensity in the region of interest (ROI). The noise is defined as the root mean square (RMS) signal intensity in an ROI outside of the material to be tested.

Medical robotic systems that are suitable in MRI-environment have been reported so far [1,10-20] and a review of the deteriorations which these robotic systems create in the SNR of an MR image are discussed. The robotic systems are mainly systems for prostate interventions using needle [10-12], surgical assisted robots [1,13], surgical robot for deep brain stimulation [14], image guided interventions [15],

diagnostic and therapeutic interventions in the abdominal and thoracic cavities [16], heart diseases [17] and transnasal neurosurgery [18]. Additionally, the clinical Philips Sonalleve MRgFUS system was also tested for MR compatibility [19].

The SNR according to the distance of different types of motors from the center of the MR bore was estimated [20-22]. The SNR according to the distance from the center of the MR bore of a conventional joystick was also tested and it was observed that when the joystick was placed 15 cm away from the phantom object, it did not cause any distortion to the MR image. The piezoelectric (ultrasonic) motors even that they are magnetism free, due to their operating high frequency currents can create image distortion if operated closer than 0.5 m from the image isocenter [22]. The Shinsei motors are widely used for MR compatible robotic systems [1,2,19,23-24] while Nanomotion motors are used in only few cases possible due to their high price [2,11]. However, it was resulted that as the Nanomotion motors move away from the edge RF-coil the SNR is remarkably increasing until a distance of 0.6 m while further removal does not show any change in the SNR [22]. Another important result is that with more severe operating conditions like higher voltage or higher speed, the SNR drops.

A device shall be considered as "MR compatible" if its use in the MR-environment does not adversely impact the image quality. A comparison of the SNR between three types of motors was performed [2]. It was observed that the pneumatic cylinder and controller causes no negative impact on the SNR, the Nanomotion motor slightly reduces the SNR under 3 T while under 1.5 T the reduction is significant. Pneumatic actuators are an ideal choice for MR compatibility since they are electromagnetism free, but they are hardly controllable. The Shinsei motor causes larger reduction in SNR compared to the Nanomotion motor and the pneumatic cylinder. In all cases where the Shinsei motors have been tested for MR compatibility, it was found that the SNR showed no reduction with the motors disabled whereas with the activation of the motors, the motors do not significantly affect the SNR and nor create artifacts in the MR images. In another case, the MR compatibility of the Shinsei motors was examined using FISP sequence [12]. The SNR variation of ultrasonic motor under different conditions was measured. The SNR with motor unwired had a 6.9 % reduction, with motor wired but not powered there was a slightly higher loss of SNR (7.6 %), with motor powered but not actuated a loss of 11.7 %, motor actuated at half max speed a loss of 13.8 %, and motor actuated at max speed a reduction in the SNR of 13.7 % was observed. The results using the Shinsei motors demonstrate the good compatibility of the piezo-motor with the MR-environment and consequently the piezo-motors are considered as MR compatible. Moreover, the change in the SNR by the addition of motors in MRI of 1.5 T and 3 T was compared [2]. The SNR loss is greater on 1.5 T MR scanner than on 3 T scanner.

Studies were performed to evaluate the effect of SNR after shielding the robotic device, motors and wiring of the devices [11,16,20,25]. Shielding of the electronic parts of the robotic devices improves the SNR and avoid artifacts in MR images. In a study [11], by turning the controller on with motors disabled reduced the SNR by 50 % without shielding. The SNR was reduced by 80 % without RF shielding and 40-60 % with RF shielding. In another study [20], the quality of MR image was improved by adding a shield cloth around a motor (spherical ultrasonic motor). At the center of the imaging volume the SNR without the shield was 11 while with the shield the SNR increased to 77. Shielding of the Shinsei ultrasonic motors was tested in order to achieve higher SNR in MRI-environment [16]. During the SNR measurement having a phantom inside the MRI room and when the motor was deactivated, the SNR dropped when the

unshielded motor was activated. After shielding the motor, the SNR recovered to high values.

The activation of the encoders also affects the SNR of the MR images [12,14]. Encoders are activated when the motors move in order to know when the motors should stop. Thus, encoders and motors are usually activated together to create motion of a robotic device. Despite that the motors and encoders are operated relatively close to the scanner's imaging isocenter, the system still causes negligible interference with the scanner. The success of the scanner tests described in a study [14] has shown that the sources of imaging interference produce an acceptably low contribution to SNR-variation of the imaging. Configurations were the phantom only, motor and encoder unpowered with controllers DC power supply turned on and motor running at a specific speed. The SNR with motor deactivated was improved while with motor activated there was no statistically significant variations between baseline (with phantom only) and motor running conditions. The MR compatibility of the encoders was also examined using fast low angle shot (FLASH) 2D gradient echo sequence [12]. The SNR with encoder unwired had a minor reduction of 0.4 % and with encoder wired but not powered there was a loss of 1.7 %. The SNR with encoder powered appeared a reduction of 2.6 %.

MR compatible focused transducers are constructed by companies active in the field of HIFU (Sonic Concepts, Imasonic, Biopac Systems, FUS Instruments, Medsonic). The MR compatibility of a ring transducer was examined [26]. T1 images of pork and the ring transducer during HIFU sonication showed that the noise occurred between the ring transducer and the pork. The source of noise could be the eddy current generated by the closed loop circuit like the grounding electrodes of the ring transducer. However, the MRI interference from HIFU did not occur in the ROI and the ring transducer could emit HIFU to ablate the pork as planned in the process of MR imaging. In another study, MRI-compatible HIFU system was successfully adapted to perform localized mild hyperthermia treatment in rodent models and focused transducers with sector-vortex lenses were tested for MR compatibility [27]. The effect of MR compatible focused transducers housed in ultrasound (US) probes on MRI monitoring were evaluated [28]. It was found that MR compatible US probes with backing material containing a specific amount of a material (ferrite) did not disturb MR monitoring except within a few mm radius from the US probe's position. Lastly, a Sonic concepts transducer was tested for MR compatibility [29]. When the transducer was introduced in the MRI (activated) without DC supply activation, the SNR drop drastically meaning that the RF artefact of the transducer caused major artefacts despite the use of a low-pass filter.

Robotic systems, ultrasonic motors and encoders either with shielding or not were tested for MR compatibility using various MRI sequences [2,11,14-19,24,30]. Most common MR sequences that are used to monitor treatment and obtain high resolution images are the T1-weighted, T2-weighted, Spin Echo (SE), Fast Spin Echo (FSE), Gradient Echo (GRE), Fast Spoiled Gradient (FSPGR) and Echo Planar Imaging (EPI). A comparison between these common MR sequences was performed and it is concluded that they show similar SNR behavior [11,14,17-19]. A body RF-coil was used to acquire SE and GRE images of a compact linear motion stage which is actuated with ultrasonic motor [24]. The system appeared a limitation when the motor was very close to the isocenter. The limitation was that some pulse sequences (GRE, Diffusion-weighted imaging and FSE) may introduce extensive noise on the encoder signal line, resulting in device malfunction.

Materials and Methods

The 2 DOF and 4 DOF robotic systems were tested for MR compatibility. The axes of the robotic devices were driven by piezoelectric ultrasonic motors (USR30-S3 N, Shinsei Kogyo Corp., Tokyo, Japan). For each DOF, an angular optical encoder was used (EM1-2-2500-I EM1, US Digital Corporation, Vancouver, WA 98684, USA).

The SNR was measured in an agar-based phantom (6 % w/v agar, 30 % v/v evaporated milk) for amplifier and transducer activation and the SNR was also measured for different configurations (robotic device in MR bore, connection of robotic device with piezoelectric motors and optical encoders and activation of these devices) in an MR-phantom (cylindrical, SNR 150027). The FUS system was consisted by a signal generator (HP 33120A, Agilent Technologies, Englewood, CO, USA), an RF amplifier (250 W, AR, Souderton, PA, USA) and a spherical transducer (Medsonic LTD). The transducer operates at 2.6 MHz, has focal length of 6.1 cm and diameter of 3.8 cm.

The robotic FUS systems were tested in a 1.5 T MR system (Signa, General Electric, Fairfield, CT, USA) using a GPFLEX coil (USA instruments, Cleveland, OH, USA). Figure 1 shows the experimental set-up with the transducer and the agar-based phantom on the table of the GE MRI scanner that was used to test the MR compatibility of the transducer (activated or not) and the SNR effect after amplifier activation. Figure 2 illustrates the experimental set-up with the 2 DOF robotic device and the MR-phantom in the MRI room but outside the MR bore. Figure 3 shows the experimental set-up after it was placed in the MR bore. The RF-coil was placed around the agar-based phantom in order to enhance the MR signal.

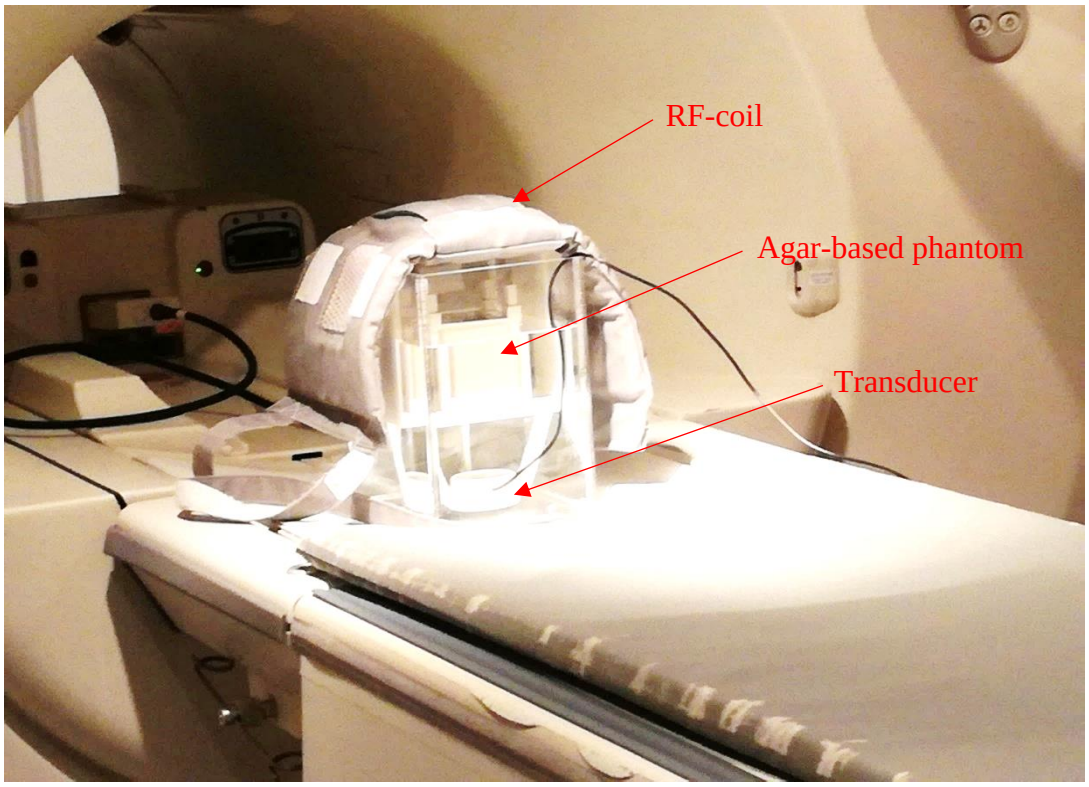

Figure 1: Experimental set-up to check the MR compatibility of the transducer and amplifier activation.

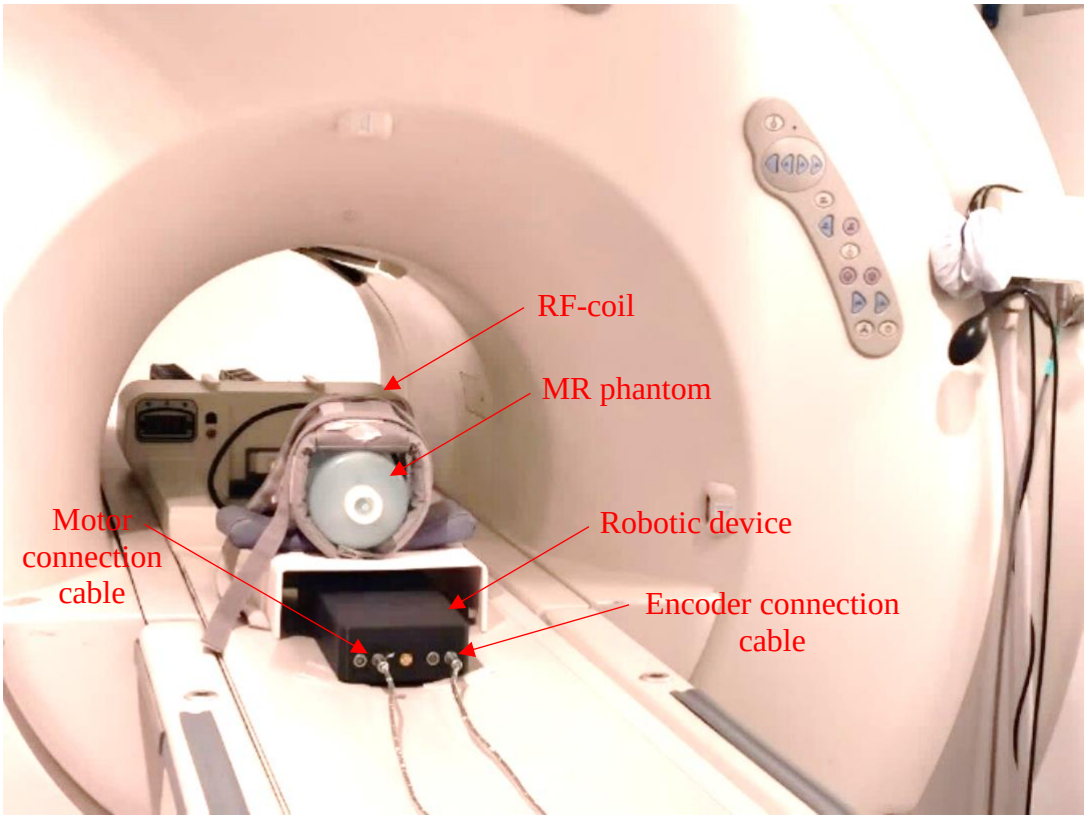

Figure 2: Experimental set-up as illustrated in the MRI room but outside the MR bore in order to check the MR compatibility of the piezoelectric motors and optical encoders. The 2 DOF robotic system was used.

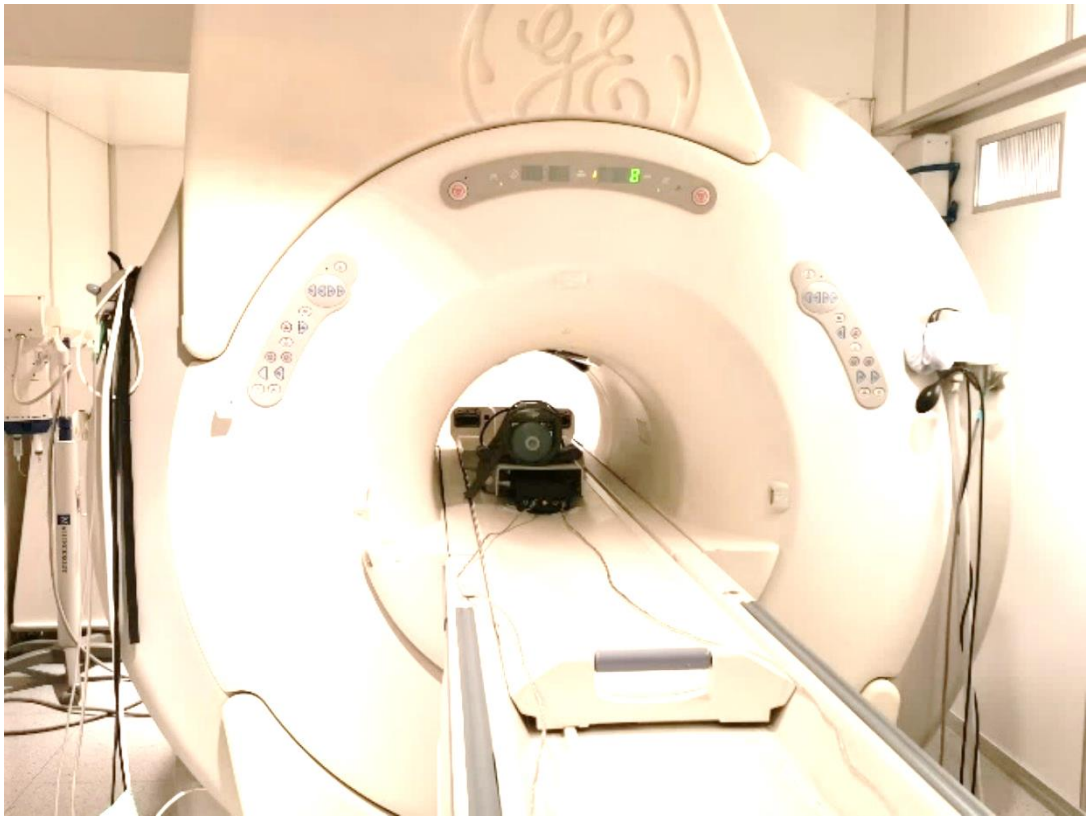

Figure 3: Experimental set-up as illustrated in the MR bore in order to check the MR compatibility of the piezoelectric motors and optical encoders. The 2 DOF robotic system was used.

MR compatibility of the transducer

In order to test the MR compatibility of the activation of the transducer and amplifier the agar-based phantom was used. The SNR was measured under various conditions (electronic system presence or activation, and transducer presence or activation) using T1W-SPGR with the following parameters: repetition time (TR) = 40 ms, echo time (TE) = 19 ms, field of view (FOV) = 21 cm, matrix = 128 × 128, flip angle = 30^{o} , Number of excitations (NEX) = 1. Table 1 summarizes the different conditions for which the SNR of the agar-based phantom was calculated.

Table 1: List of the different conditions for which the SNR of the agar-based phantom was measured in order to evaluate the MR compatibility of the transducer.

Nº	Condition
1	Transducer and amplifier deactivated
2	Transducer deactivated and amplifier activated
3	Amplifier activated and transducer activated at 12 s
4	Amplifier activated and transducer activated at 24 s
5	Amplifier activated and transducer activated at 36 s
6	Amplifier activated and transducer activated at 48 s
7	Amplifier activated and transducer activated at 60 s

An axial T2W-FSPGR image of the experimental set-up was initially obtained as shown in Figure 4. The following parameters were used: repetition time (TR) = 5 ms, echo time (TE) = 1.4 ms, field of view (FOV) = 21 cm, matrix = 256 × 256, flip angle = 30^{o}, Number of excitations (NEX) = 1. Coronal MR images of the agar-based phantom taken with T1W-SPGR sequence are shown in Figure 5 for the different conditions of Table 1. Figure 5A, shows the SPGR image of the phantom with the transducer placed in the MRI bore and deactivated and the amplifier unpowered. Figure 5B, shows the SPGR image of the phantom after powering on the amplifier, but with deactivation of the transducer. Figures 6C, D, E, F and G show the SPGR images of the phantom with activation of the transducer at different sonication time during a total sonication of 60 s.

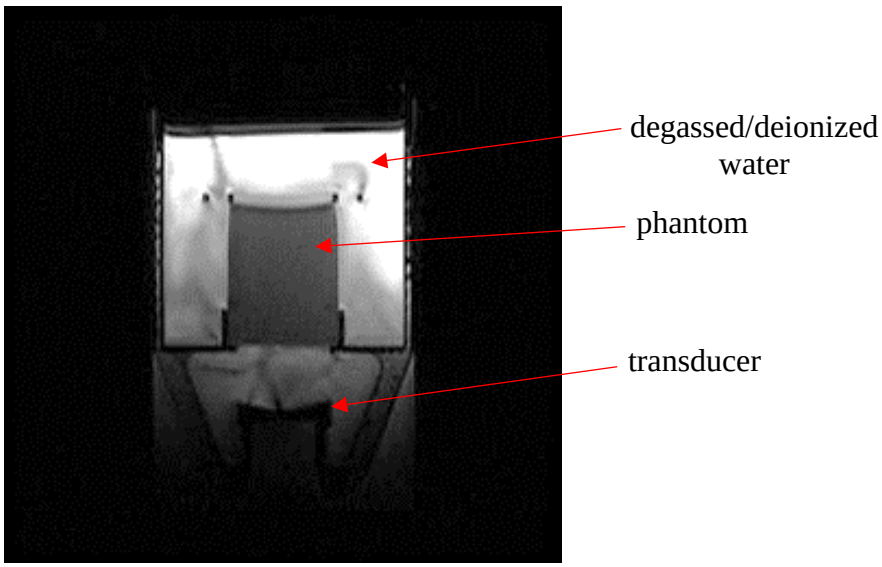

Figure 4: T2W-FSPGR coronal image of the experimental set-up that was used to investigate the MR compatibility of the transducer.

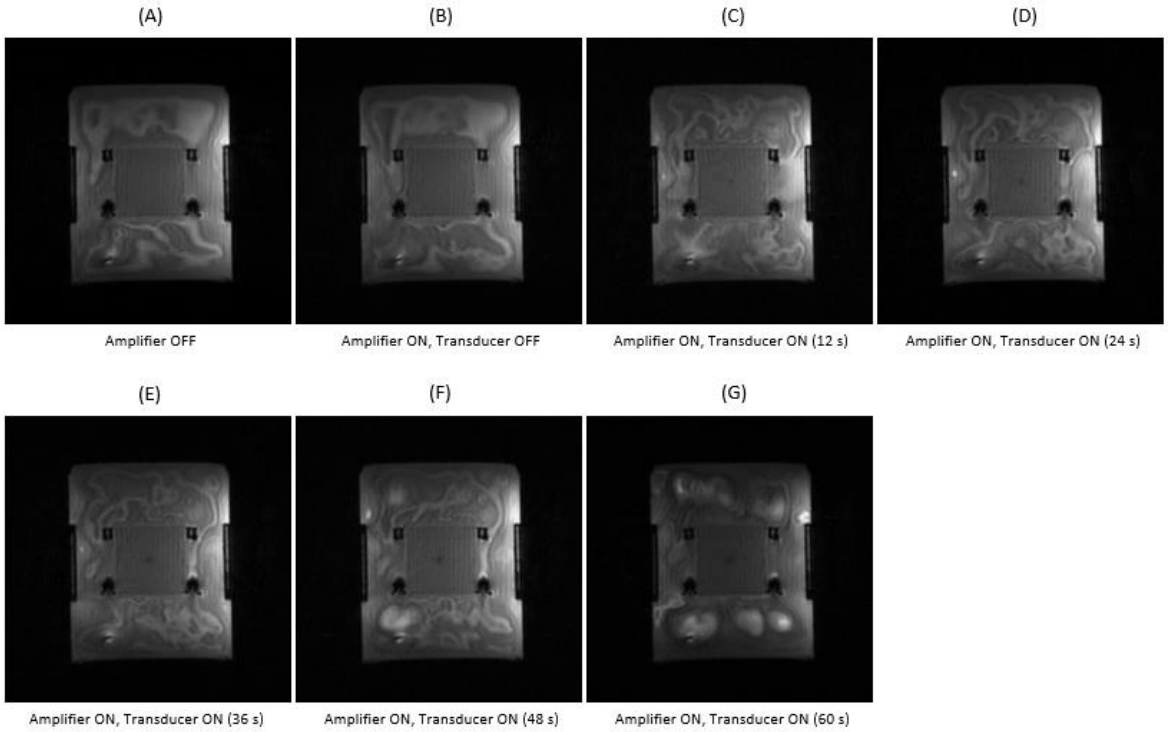

Figure 5: Coronal MR images obtained using T2W-SPGR sequence for A) amplifier without DC supply, B) amplifier with DC supply and transducer deactivated, C) amplifier with DC supply and transducer activated at 12 s, D) 24 s, E) 36 s, F) 48 s, and F) 60 s .

The difference between the MR image obtained with the amplifier unpowered and after the activation of the amplifier is shown in Figure 6. The pixel-by-pixel of the MR image obtained with the amplifier powered and transducer deactivated (reference image) was subtracted from the MR images taken with the transducer activated at 12 s, 24 s, 36 s, 48 s, and 60 s as shown in Figure 7. The surrounding area of the phantom is the degassed/deionized water which was vibrated by the activation of the transducer.

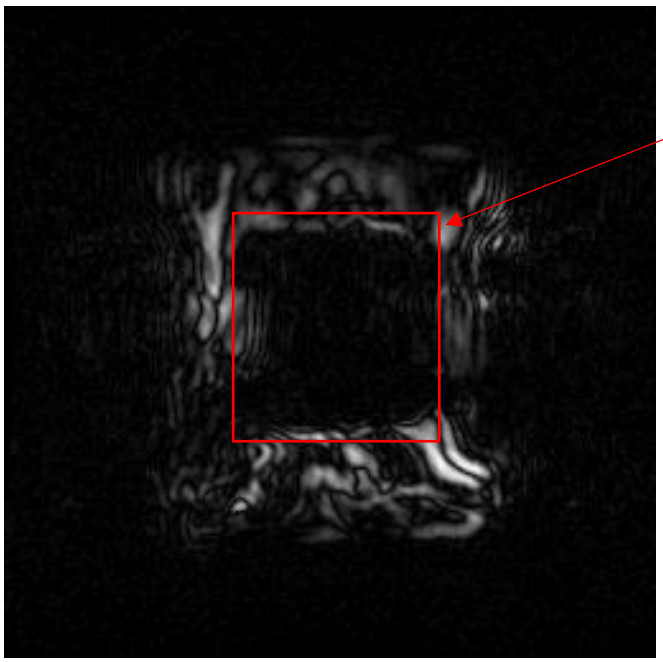

Figure 6: Difference image between the MR image obtained with the amplifier deactivated and the MR image obtained after powering on the amplifier.

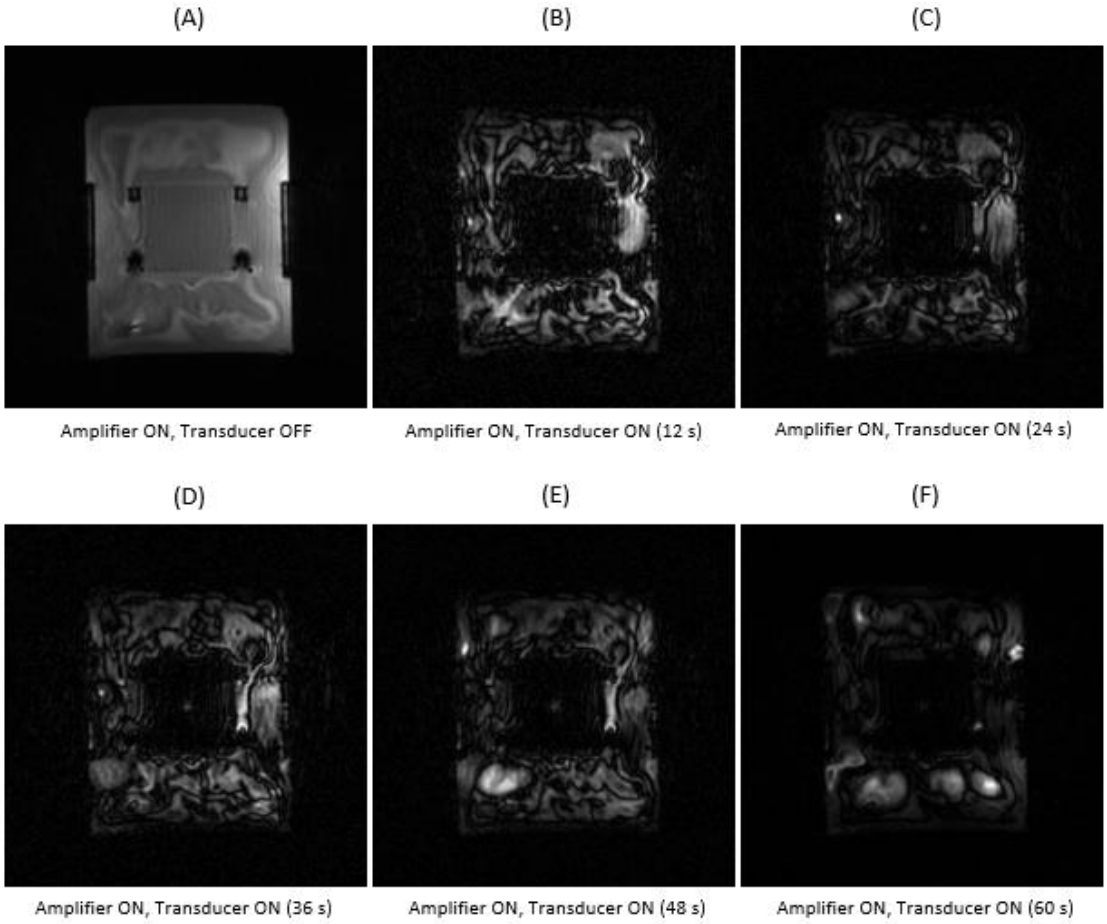

Figure 7: Difference images between the MR image obtained with the amplifier powered and transducer deactivated (A) and MR images taken with the transducer activated at 12 s, 24 s, 36 s, 48 s, and 60 s.

A method in NEMA standard [9] was used to measure the SNR in the phantom for different configurations. A measurement ROI of at least 75 % of the area of the image of the signal-producing volume of the phantom was selected. The SNR was calculated by subtracting the mean signal of that ROI from the standard deviation of the same area (in pixels) in the background of the image (noise) as shown in equation (1).

$$SNR = \frac{S_{image}}{SD_{background}} \quad (1)$$

Figure 8 shows the SNR measured for different activations (amplifier and transducer) using T1W-SPGR. The amplifier ON means that the RF amplifier was activated with a DC supply and the transducer ON means that the transducer was activated and sonicated HIFU energy in the agar-based phantom. When the transducer was not activated without DC supply activation, the SNR was high. When the amplifier was powered on, the SNR dropped slightly meaning that the RF amplifier does not cause artefacts to the MR images and it has minimal effect on the SNR. The SNR decreased drastically when the transducer was activated. During transducer's activation, the SNR remained almost constant meaning that the duration of the activation of the transducer does not affect the SNR.

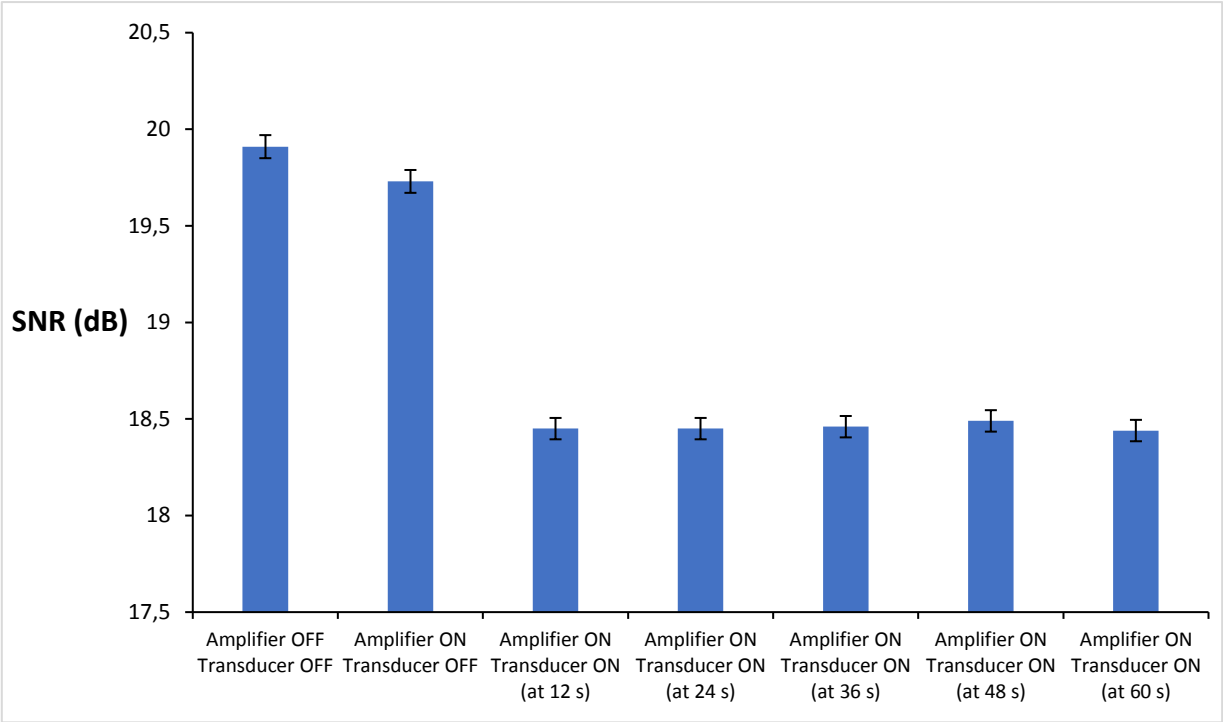

Figure 8: SNR using T1W-SPGR sequence measured for different activation conditions (RF amplifier and transducer).

MR compatibility of the robotic devices, ultrasonic piezoelectric motors and optical encoders

MR images of different pulse sequences were acquired. A T2-Fast Recovery Fast Spin Echo (T2W-FRFSE) sequence was used as a high-resolution image of the different conditions. The MR thermometry sequences Fast Spoiled Gradient (FSPGR) and Echo Planar Imaging (EPI) were also obtained and the SNR for the different conditions was compared. Table 2 summarizes the MR pulse sequences used and the different conditions for which the SNR was calculated in order to estimate the SNR of the MR quality assurance phantom. Since during imaging the positioning device is static, the piezoelectric motor was deactivated in all the tests. The electronic system that controls the piezoelectric motor and the optical encoder required DC electricity.

Table 2: List of MR sequences and conditions that were used to calculate SNR.

Nº	MR sequences
1	T2W-FRFSE
2	FSPGR
3	EPI
	Conditions
1	Phantom only (baseline image)
2	Robotic device in MR bore (unconnected)
3	Robotic device in MR bore (connected) with electronic system deactivated
4	Robotic device in MR bore (connected) with electronic system activated

MR images of the cylindrical phantom taken with T2W-FRFSE, FSPGR and EPI are shown for the different conditions in Figures 9, 10 and 11 respectively. The

difference between the baseline image (with phantom only) and the image taken in each different condition is also shown.

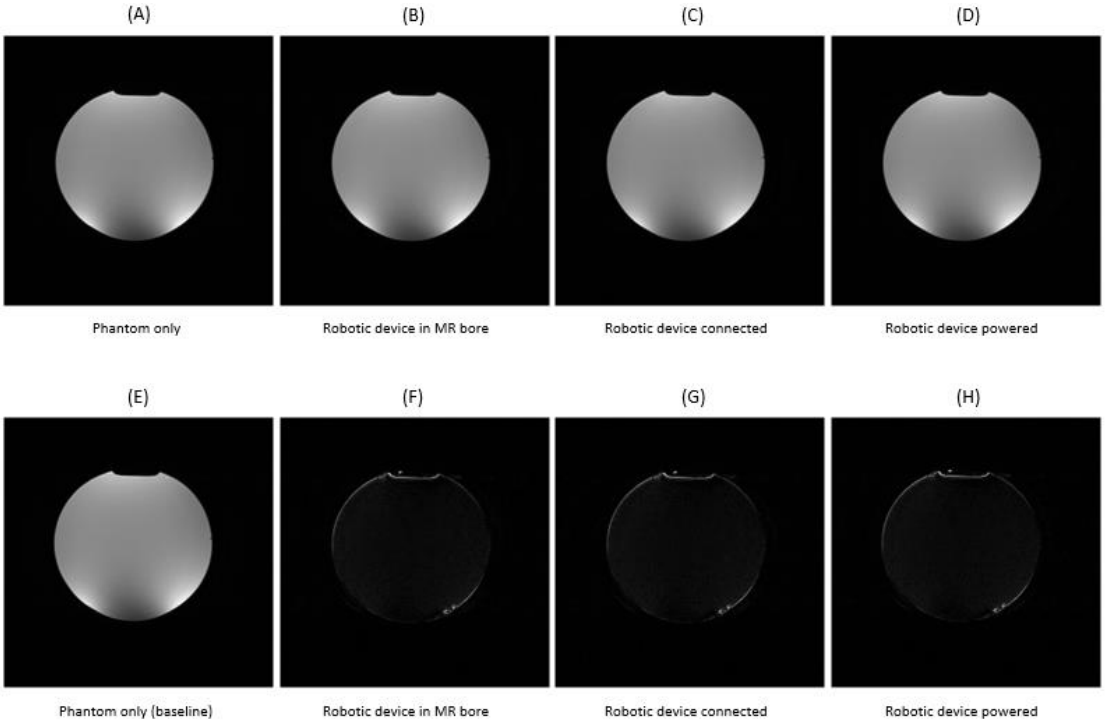

Figure 9: MR images (top) obtained using T2W-FRFSE sequence for the different conditions and the corresponding differences (bottom) between each condition and the baseline (phantom only) image.

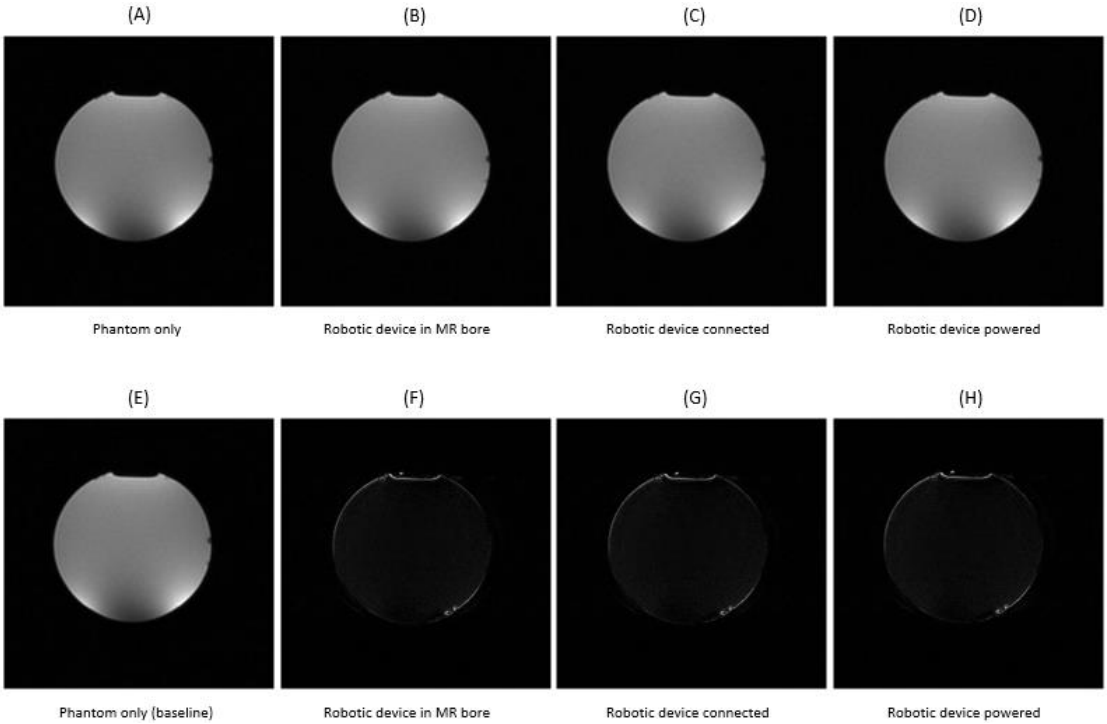

Figure 10: MR images (top) obtained using FSPGR sequence for the different conditions and the corresponding differences (bottom) between each condition and the baseline (phantom only) image.

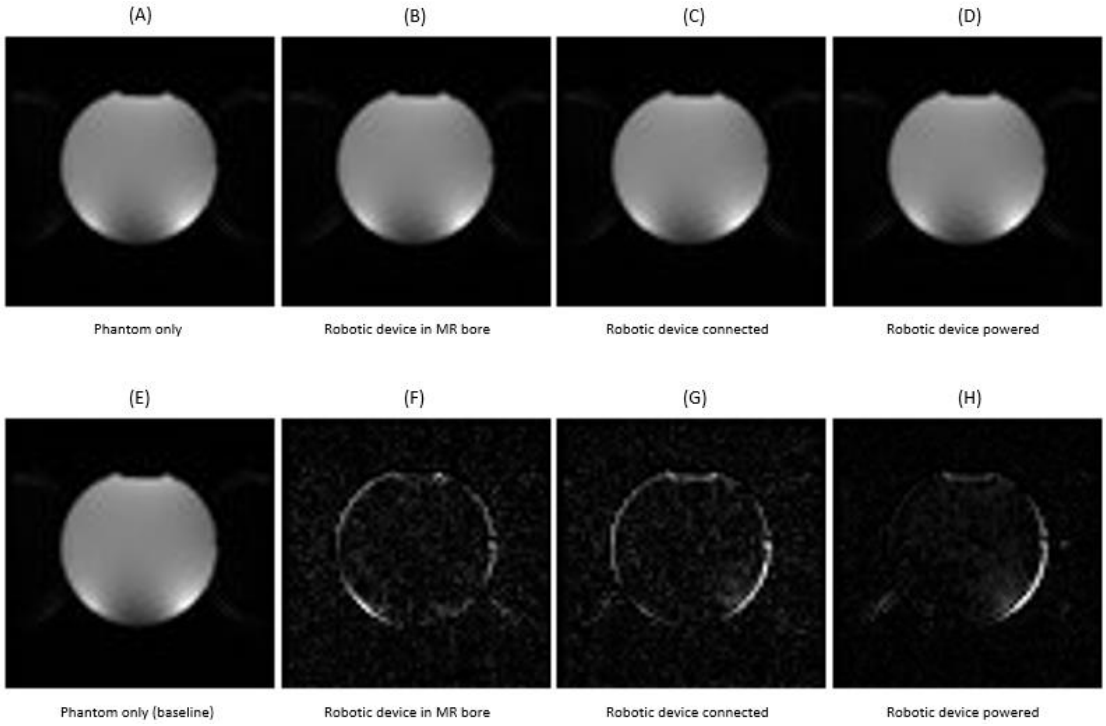

Figure 11: MR images (top) obtained using EPI sequence for the different conditions and the corresponding differences (bottom) between each condition and the baseline (phantom only) image.

Figures 12, 13 and 14 show the SNR measured for different conditions using T2W-FRFSE, FSPGR and EPI respectively.

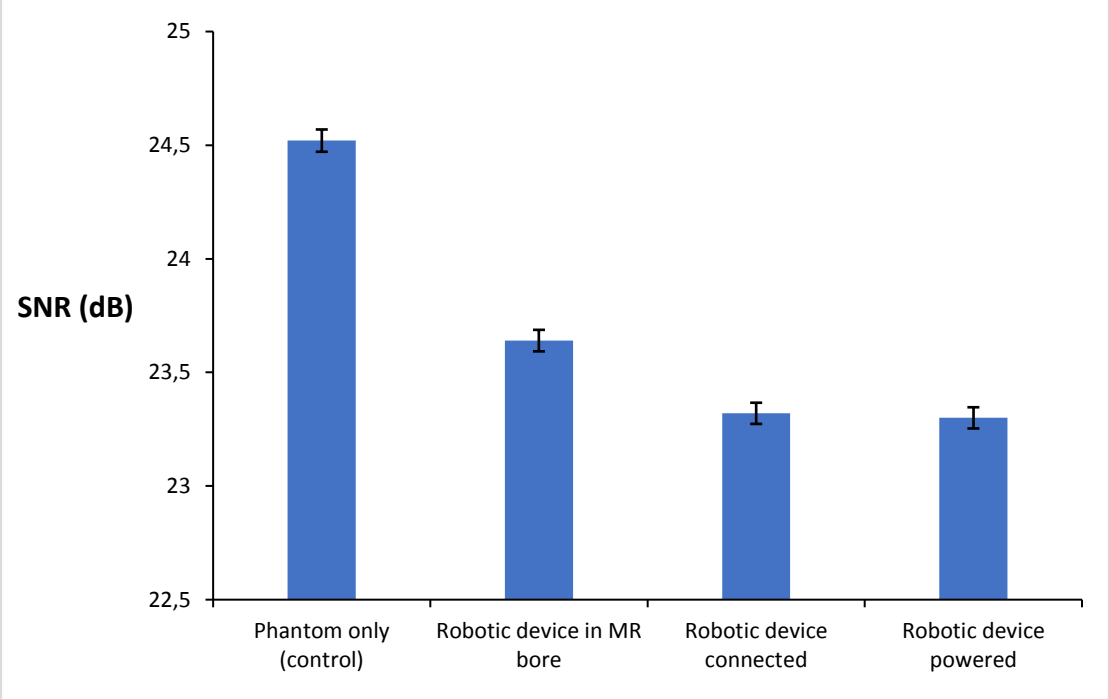

Figure 12: SNR using T2W-FRFSE sequence measured for different conditions.

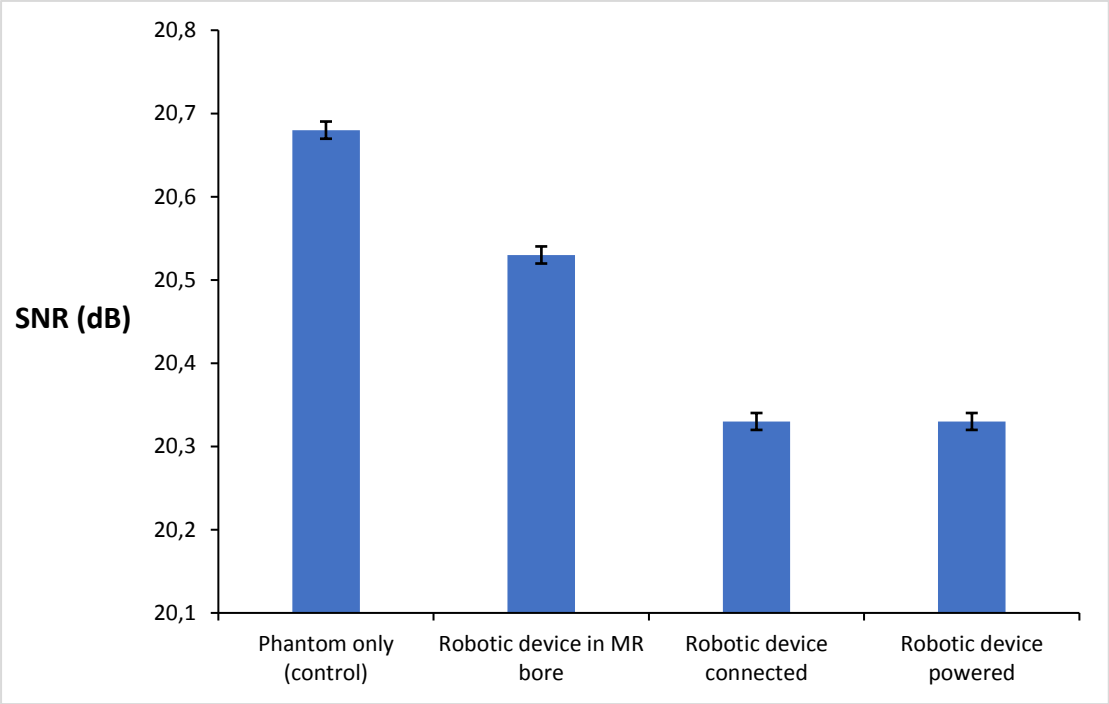

Figure 13: SNR using FSPGR sequence measured for different conditions.

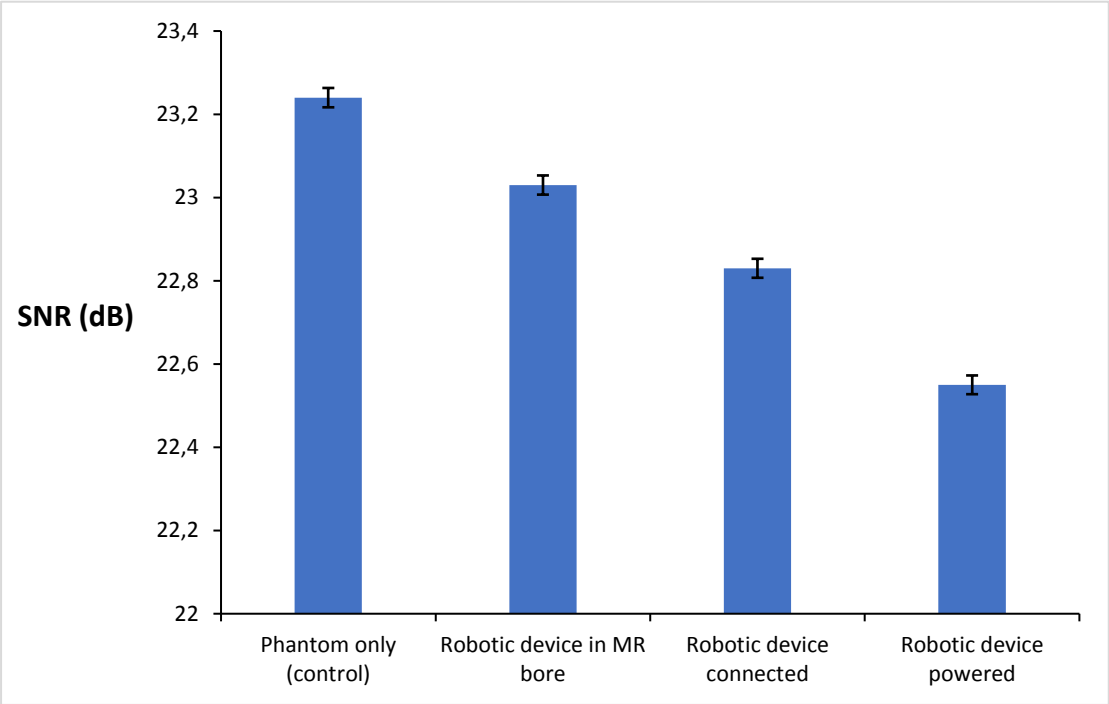

Figure 14: SNR using EPI sequence measured for different conditions.

The points in the graph in Figure 15 show the SNR in the phantom for each sequence at each configuration.

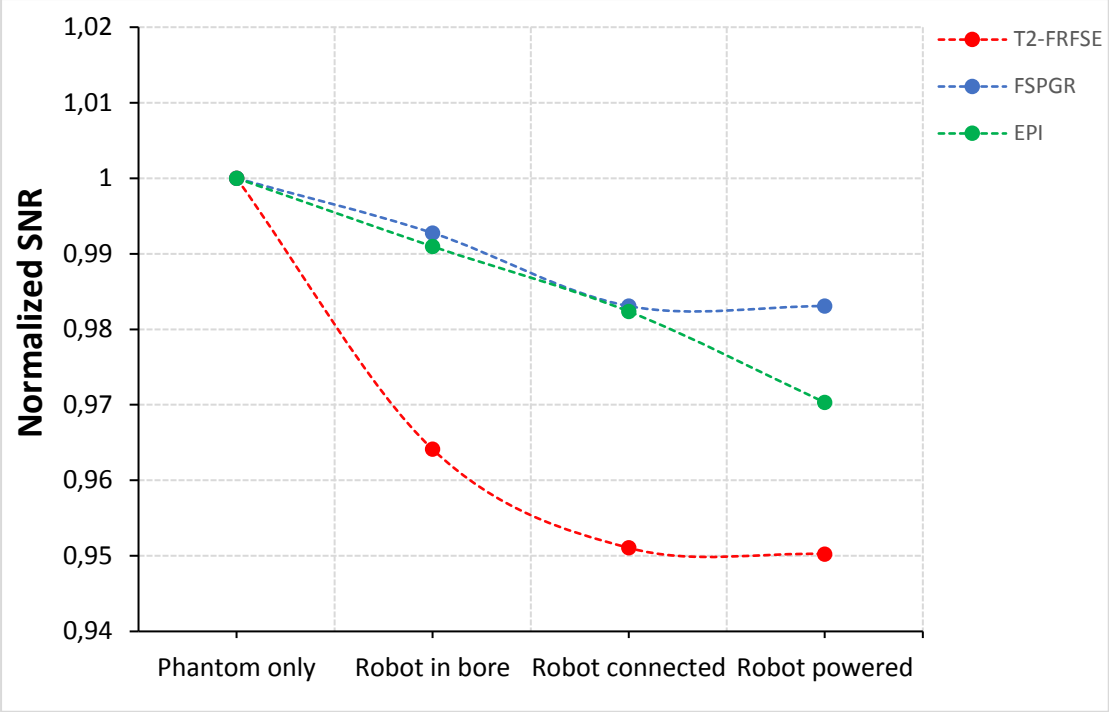

Figure 15: SNR for three MR imaging protocols with the system in different configurations. Lines represent mean SNR.

Non-Uniformity Index of agar-based phantom and MR-phantom under different configurations

The uniformity of the agar-based phantom for the different configurations was investigated. The Non-Uniformity Index (NUI) is a suitable standardized measure to investigate magnetic field uniformity. Scanning sequences, imaging planes, coils and presence of metallic materials can influence MR image uniformity. To evaluate the uniformity of the images, we measured the signal intensity at 5 sample points according to the standardized sample method laid out by NEMA (Figure 16) which allows for successive calculation of an NUI for each image. The 5-point measurement was used for each different configuration in order to investigate if the different conditions of the robotic system affected the uniformity of the phantom. Figure 17 shows the NUIs (in %; lower means more uniform) based on 5 sampling points for the different configurations.

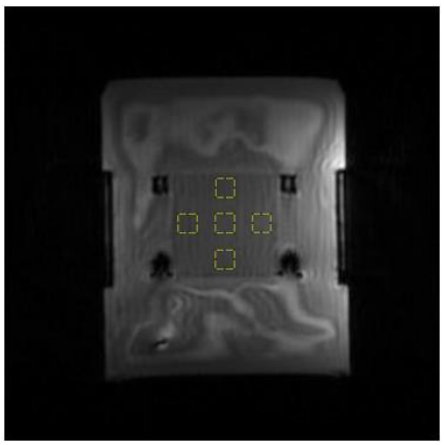

Figure 16: Standardized 5-point measurement method based on NEMA in order to calculate the NUI of the agar-based phantom for the different configurations.

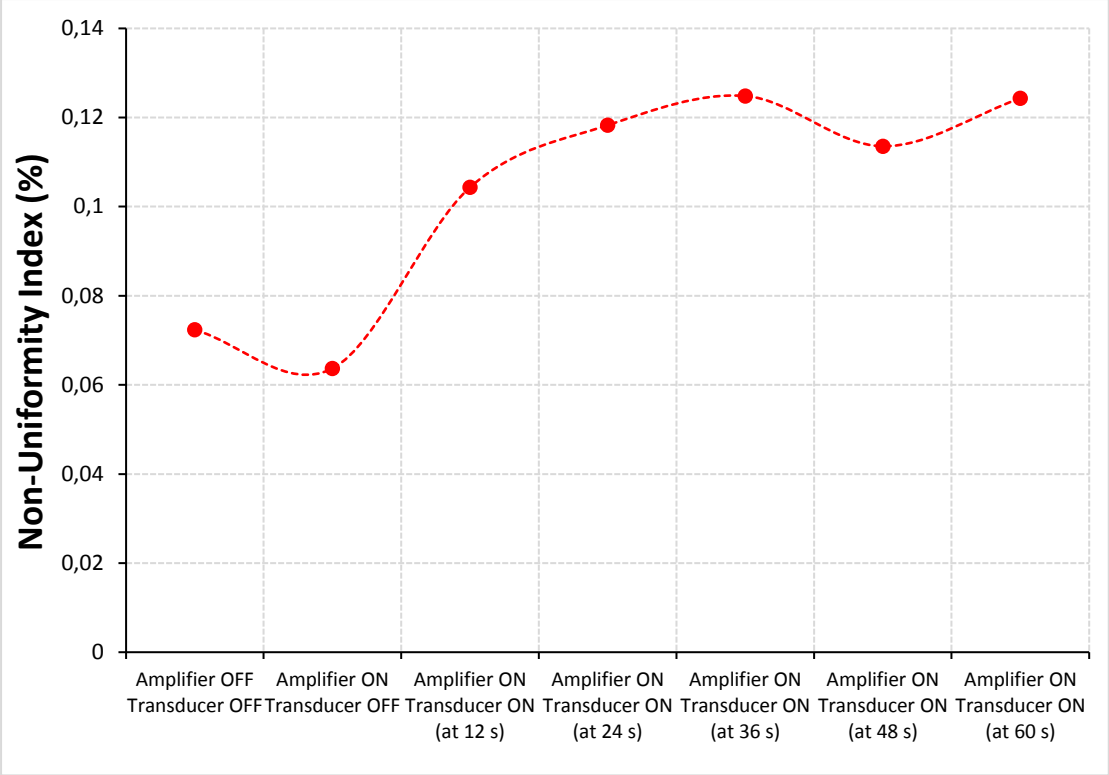

Figure 17: NUI versus different configurations using T1W-SPGR sequence for the agar-based phantom.

The 5-point measurement was also used for each different configuration and MR sequence (presence of the robotic devices, motors and encoders) for the MR quality assurance phantom. Figure 18 shows the standardized sample method laid out by NEMA in order to calculate the NUI of the MR quality assurance phantom for the different configurations. Figure 19 shows the NUIs based on 5 sampling points for the different MR sequences and configurations.

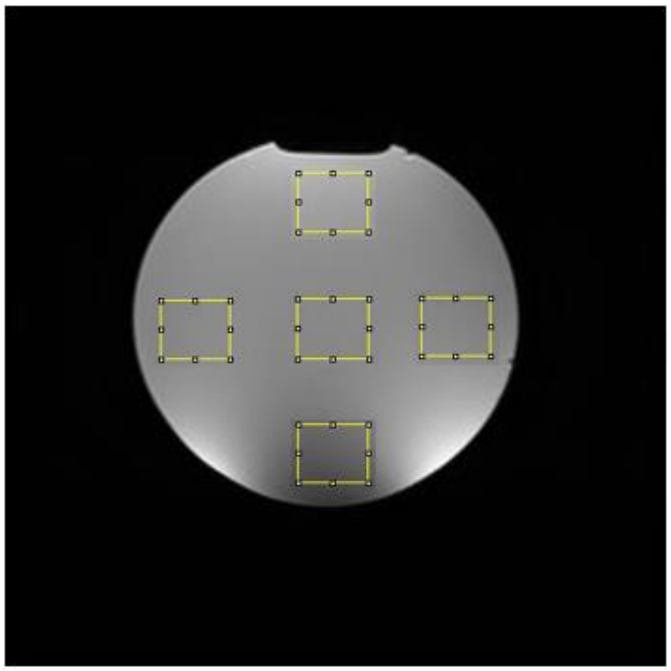

Figure 18: Standardized 5-point measurement method based on NEMA in order to calculate the NUI of the MR quality assurance phantom for the different configurations.

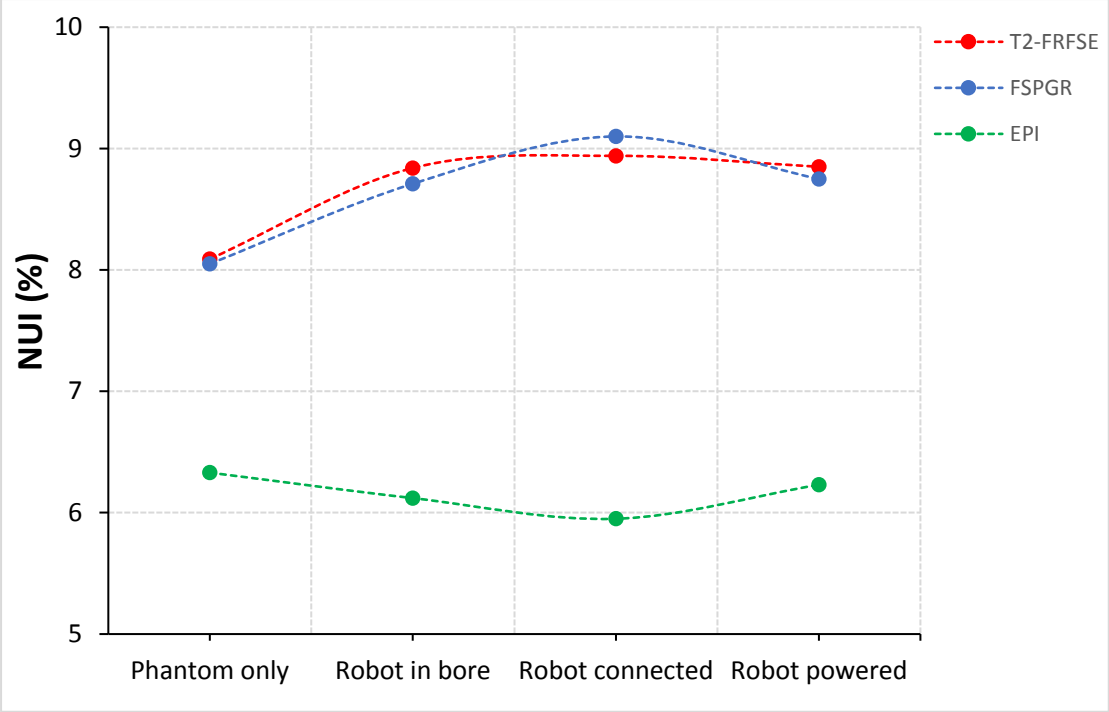

Figure 19: NUI versus condition for three MR sequences obtained in the MR quality assurance phantom.

Conclusions

In this deliverable, the MR compatibility of the activation of the transducer and RF amplifier was evaluated in an agar-based phantom. The SNR was measured under various conditions (electronic system presence or activation, and transducer presence or activation) using T1W-SPGR sequence. The SNR was maximum when all components were deactivated. There was some decrease in the SNR when the RF amplifier was activated and there was a higher decrease in the SNR when the transducer was activated. During transducer's activation, the SNR remained almost constant meaning that the duration of the activation of the transducer does not affect the SNR.

We have shown that the piezoelectric motors and optical encoders of the robotic devices to be MR compatible under high resolution sequences and MR thermometry imaging sequences. The SNR in the MR quality assurance phantom for different configurations was calculated. There was some decrease in the SNR when a motor or encoder or the transducer was activated. It was shown that the SNR does not change dramatically from the control condition with the phantom present in the MR bore or with the presence of the electronic system (activated or not). The highest reduction of the SNR was calculated with T2W-FRFSE sequence and there was a reduction of around 1.2 dB. The SNR using FSPGR and EPI dropped slightly with each configuration change. Both motors and encoders did not cause dramatic reduction in the SNR for all MR sequences. The overall result is that both FSPGR and EPI can be used to obtain MR data for MR thermometry since the robotic system does not significantly affect the SNR. However, an attempt to obtain MR images during motion of the robotic system introduced extensive noise on the encoder signal line, resulting in device malfunction. **Anyway, imaging during robot motion is never needed and therefore this unpleasant situation does not affect any of the imaging sequences.**

The NUI of the agar-based phantom under various conditions was estimated. The uniformity of the agar-based phantom was slightly improved when the amplifier was activated while the uniformity was decreased when the transducer was activated. During the activation of the transducer, the uniformity of the phantom remained almost stable without significant changes.

The NUI of the MR quality assurance phantom for the different MR sequences and configurations was also calculated. At the control condition with the phantom only, the minor drop in the uniformity of the phantom was possibly due to the poor transmission of the RF-coil. The uniformity of the phantom showed the same behavior for the T2W-FRFSE and FSPGR sequences. It was slightly decreased when the robotic device was introduced in the MR bore and it remained almost unaffected when the robotic device was connected and activated. The uniformity of the phantom using the EPI sequence was better than using T2W-FRFSE or FSPGR sequences and did not show any drop during the different configurations. Overall, the presence of the robotic device in the MR bore, its connection to the electronic system and the activation of the electronics did not significantly affect the SNR and uniformity of the MR-phantom.

To sum up, the activation of the amplifier, transducer, piezoelectric motors and optical encoders does not affect the quality of MR thermometry. Since the quality of the MR images is not affected more than expected, electromagnetic shielding is not necessary.

References

[1] Chinzei, K., Hata, N., Jolesz, FA., Kikinis, R. MR compatible surgical assist robot: system integration and preliminary feasibility study. In: Delp, SL., DiGoia, AM., Jaramaz, B., editors. MICCAI 2000. LNCS. Vol. vol. 1935. Springer: Heidelberg, 2000. P. 921-933.

[2] Gregory S. Fischer, Axel Krieger, Iulian Iordachita, Csaba Csoma, Louis L. Whitcomb, and Gabor Fichtinger. MRI Compatibility of Robot Actuation Techniques-A Comparative Study. Med Image Comput Comput Assist Interv. 2008; 11 (Pt 2): 509-517.

[3] L. Bendel. The effect of mechanical deformation on magnetic properties of MRI artifacts of type 304 and 316L stainless steel. J. Magn. Reason. Imaging 7, 1190-1173 (1997).

[4] Damianou C, Giannakou M, Yiallouras C, Menikou G. The role of three-dimensional printing in magnetic resonance imaging-guided focused ultrasound surgery. Digit Med 2018; 4: 22-6.

[5] R. Chopra, L. Curiel, R. Staruch, L. Morrison, and K. Hynynen. An MRI-compatible system for focused ultrasound experiments in small animal models. Med. Phys. 36, 1867-1874 (2009).

[6] C. Yiallouras and C. Damianou. Review of MRI positioning devices for guiding focused ultrasound systems. Int. J. Med. Rob. Comput. Assisted Surg. 11, 247-255 (2015).

[7] FDA. Establishing safety and compatibility of passive implants in the magnetic resonance (MR) environment. Technical Report, Food and Drug Administration, 2014.

[8] ASTM. Standard practice for marking medical devices and other items for safety in the magnetic resonance environment. Technical Report ASTM F2503-13, ASTM International, West Conshohocken, PA, 2013.

[9] The Association of Electrical and Medical Imaging Equipment Manufacturers: Determination of Signal-to-Noise-Ratio (SNR) in Diagnostic Magnetic Resonance Imaging. NEMA Standard Publication MS 1-2008.

[10] Dan Stoianovici, Danny Song, Doru Petrisor, Daniel Ursu, Dumitru Mazilu, Michael Mutener, Michael Schar, and Alexandru Patriciu. "MRI Stealth" robot for prostate interventions. Minim Invasive Ther Allied Technol, 2007; 16(4): 241-248.

[11] Axel Krieger, Sang-Eun Song, Nathal B. Cho, Iulian Iordachita, Peter Guion, Gabor Fichtinger, and Louis L. Whitcomb. Development and Evaluation of an Actuated MRI-Compatible Robotic System for MRI-Guided Prostate Intervention. IEEE ASME Trans Mechatron, 2012 September 12; 18(1): 273-284.

[12] Haytham Elhawary, Aleksander Zivanovic, Marc Rea, Brian Davies, Collin Besant, Donald McRobbie, Nandita de Souza, Ian Young, and Michael Lamperth. The

Feasibility of MR-Image Guided Prostate Biopsy Using Piezoceramic Motors Inside or Near to the Magnet Isocentre. MICCAI 2006, LNCS 4190, pp. 519-526.

[13] Juha Harja, Jussi Tikkanen, Hannu Sorvoja, and Risto Myllyla. Magnetic resonance imaging-compatible, three-degrees-of-freedom joystick for surgical robot. Int J Med Robotics Comput Assist Surg 2007; 3: 365-371.

[14] Yi Wang, Gregory A. Cole, Hao Su, Julie G. Pilitsis and Gregory S. Fischer. MRI Compatibility Evaluation of a Piezoelectric Actuator System for a Neural Interventional Robot. 31st Annual International Conference of the IEEE EMBS, 2009.

[15] Ankur Kapoor, Brad Wood, Dumitru Mazilu, Keith A. Horvath, and Ming Li. MRI-compatible Hands-on Cooperative Control of a Pneumatically Actuated Robot. IEEE Int Conf Robot Autom, 2009 July 6; 2009: 2681-2686.

[16] Nikolaos V. Tsekos, Alpay Ozcan, and Eftychios Christoforou. A Prototype Manipulator for Magnetic Resonance-Guided Interventions Inside Standard Cylindrical Magnetic Resonance Imaging Scanners. Journal of Biomechanical Engineering, Vol. 127, November 2005.

[17] Fujio Tajima, Kousuke Kishi, Kouji Nishizawa, Kazutoshi Kan, Yasuhiro Nemoto, Haruo Takeda, Shin-ichiro Umemura, Hiroshi Takeuchi, Masakatsu G. Fujie, Takeyoshi Dohi, Ken-ichi Sudo, and Shin-ichi Takamoto. Development of MR Compatible Surgical Manipulator toward a Unified Support System for Diagnosis and Treatment of Heart Disease. MICCAI 2002, LNCS 2488, pp. 83-90.

[18] Yoshihiko Koseki, Toshikatsu Washio, Kiyoyuki Chinzei, and Hiroshi Iseki. Endoscope Manipulator for Trans-nasal Neurosurgery, Optimized for and Compatible to Vertical Field Open MRI. MICCAI 2002, LNCS 2488, pp. 114-121.

[19] Karl D. Price, Vivian W. Sin, Charles Mougenot, Samuel Pichardo, Thomas Looi, Adam C. Waspe, and James M. Drake. Design and validation of an MR-conditional robot for transcranial focused ultrasound surgery in infants. Med. Phys. 43 (9), September 2016.

[20] T. Mashimo and S. Toyama. MRI-Compatibility of a Manipulator using a Spherical Ultrasonic Motor. 12th IFToMM World Congress, Besancon (France), June 18-21, 2007.

[21] Hempel E, Fischer H, Gumb L, Hohn T, et al. An MRI-compatible surgical robot for precise radiological interventions. Computer Aided Surgery, 2003; 8: 180-191.

[22] Roger Gassert, Akio Yamamoto, Dominique Chapuis, Ludovic Dovat, Hannes Bleuler, and Etienne Burdet. Actuation Methods for Applications in MR Environments. Magnetic Resonance Engineering, 2006, Vol 29B(4): 191-209.

[23] Valentina Hartwig, Nicola Vanello, Giuseppe Gaeta, Nicola Sgambelluri, Enzo Pasquale Scilingo, Antonio Bicchi. Design of fMRI Compatible Actuators. TOUCH-HapSys.

[24] Mohammad Ali Tavallaei, Patricia M. Johnson, Junmin Liu, and Maria Drangova. Design and evaluation of an MRI-compatible linear motion stage. Medical Physics 43, 62 (2016).

[25] Rares Salomir, Lorena Petrusca, Vincent Auboiroux, Arnaud Muller, Maria-Isabel Vargas, Denis R. Morel, Thomas Goget, Romain Breguet, Sylvain Terraz, Jerry Hopple, Xvier Montet, Christoph D. Becker, and Magalie Viallon. Magnetic Resonance-Guided Shielding of Prefocal Acoustic Obstacles in Focused Ultrasound Therapy. Investigative Radiology, Vol 48 (6), 2013.

[26] Li-Wei Kuo, Li-Chen Chiu, Win-Li Lin, Jiun-Jung Chen, Guo-Chung Dong, Sheng-Fu Chen, and Gin-Shin Chen. Development of an MRI-Compatible High-Intensity Focused Ultrasound Phased Array Transducer Dedicated for Breast Tumor Treatment. IEEE Transactions on Ultrasonics, Ferroelectrics, and Frequency Control, vol., 65, No. 8, 2018.

[27] Chenchen Bing, Joris Nofiele, Robert Staruch, Michelle Ladouceur-Wodzak, Yonatan Chatzinoff, Ashish Ranjan & Rajiv Chopra. Localised hyperthermia in rodent models using an MRI-compatible high-intensity focused ultrasound system. International Journal of Hyperthermia, DOI: 10.3109/02656736.2015.1094833.

[28] Takashi Azuma, Kazuaki Sasaki, Ken-ichi Kawabata, Akiko Osada, Hiroyuki Itagaki, Kazumi Komura, Tetsuhiko Takahashi, Kazunari Ishida, Yutaka Satoh and Shin-ichiro Umemura. MRI-Compatible ultrasonic probe for minimally invasive therapy. IEEE Ultrasonics Symposium, 1465, 2002.

[29] Marinos Yiannakou, Georgios Menikou, Christos Yiallouras, Cleanthis Ioannides, Christakis Damianou. MRI guided focused ultrasound robotic system for animal experiments. Int. J. Med. Robotics Comput. Assist. Surg. 2017; 13:e1804.

[30] Kiyoyuki Chinzei, Ron Kikinis, and Ferenc A. Jolesz. MR Compatibility of Mechatronic Devices: Design Criteria. Medical Image Computing and Computer-Assisted Intervention-MICCAI 1999, pp. 1020-1030.